Hypothesis

Repair and Misrepair of Telomeric DNA in Dynamic Interactions with PML Nuclear Bodies and Lamin B1—A Gear-Wheel Nuclear Traffic.

Kristine Salmina , Fēlikss Rūmnieks , Dace Pjanova , Jekaterina Erenpreisa *

Posted Date: 5 January 2024

doi: 10.20944/preprints202401.0111.v2

Keywords: Cancer; cellular senescence; telomere attrition; alternative telomere lengthening; PML nuclear bodies; lamin B1; ALU; surface heterochromatin; nuclear rotation; chromothripsis

Hypothesis

Repair and Misrepair of Telomeric DNA in Dynamic Interactions with PML Nuclear Bodies and Lamin B1—A Gear-Wheel Nuclear Traffic

Kristine Salmina [1], Felikss Rumnieks [1], Dace Pjanova D [1,2] and Jekaterina Erenpreisa [1,*]

[1] Latvian Biomedicine Research and Study Centre, LV-1067 Riga, Latvia; salmina.kristine@gmail.com (K.S.); felikss.rumnieks@biomed.lu.lv (F.R.)
[2] Riga Stradins University, Dzirciema 16, LV-1007 Riga, Latvia; dace@biomed.lu.lv (D.P.)
* Correspondence: katrina@biomed.lu.lv

Abstract: Telomeres in epithelial tumours are usually maintained by telomerase, however, in the breast cancer MDA-MB-231 cell line, polyploid cells, induced by doxorubicin (DOX) were found, after mitotic slippage, transiently shifting to recombinatory alternative telomere lengthening (ALT) in PML bodies (APBs). The involvement of the meiotic recombination proteins was evidenced here by juxta-co-localisation of SPO11, DMC1 and RAD51/γH2AX with APBs in these and melanoma SkMel28-DOX-treated cells. Using sublethal doses of DOX we also observed the formation of the PML dimeric rod tandems linking γH2AX/TRF2 foci into ribbons discontinuously inserted into lamin B1 and circumventing cell nuclei. Next, we link these PML-lamin B1 insertions and peripheral rotation of the tandemly linked telomere repeats with the mobility of the nuclear envelope limited chromatin sheets (ELCS). ELCSs comprise two layers of the criss-crossed ~30 nm granules derived from surface heterochromatin (epichromatin) which contains telomere repeats enriched in GpC, PML, and ALU. ELCS protrude, circumvent, loop, split, fuse, and rejoin polyploid cell nuclei. We propose this gear-wheel-like turnover of telomere repeats to be used for the homology search. Interstitial and end-telomere repeats flanked by fragile ALU-Z flipons become recognised by SPO11 nuclease, attract TRF2, PML, and meiotic recombinases. Subsequently, they perform ALT recombining subtelomeres and telomeres or undergo non-homologous end-joining and chromosome rearrangements with ELCS. This mechanism increases the chance of cell survival and may be involved in chromothripsis.

Keywords: cancer; cellular senescence; telomere attrition; alternative telomere lengthening; PML nuclear bodies; lamin B1; ALU; surface heterochromatin; nuclear rotation; chromothripsis

1. Introduction

Accelerated cell senescence (ACS) imposed by oncogenes, oxidative stress and drug treatments on cancer cells [1] is characterised by interruption of proliferation, telomere attrition [2,3], degradation of lamin B1 [4–6], activation of transposable elements [7] and the transition by mitotic slippage (MS) to reversible polyploidy, as well [8–10].

Paradoxically, ACS also serves and even is needed for reprogramming [11], cancer cell stemness [12], and drug-resistant cell survival [13–15]. Usually, telomeres are maintained in epithelial tumours by telomerase (reverse transcription mechanism), however 10-15% of tumours, mostly mesenchymal, support telomere length by alternative mechanism based on telomere recombination aided by promyelocyte leukaemia PML bodies, both mechanisms can coexist [16]. In our previous article [10], on triple-negative breast cancer MDA MB 231-doxorubicin-treated (MDA-DOX) cells underwent mitotic slippage (MS) revealing senescence and DNA damage in most cells lasting for three weeks (Figure 1 A-D). During MS resulting in polyploidisation, the cells cast off telomere ends, shelterin TRF2 (Figure 1A, B), telomerase and were transiently undergoing the alternative telomere lengthening (ALT) in PML bodies (APB) [10]. Nevertheless, three weeks later, the telomerase activity was restituted in the clones of the recovered depolyploidised survivors, resuming mitotic divisions (Figure 1C). Interestingly, in this interim ALT-period, we found by qPCR upregulation of several proteins of meiotic prophase, particularly high of the DNA recombination-related nuclease SPO11

 doi:10.20944/preprints202401.0111.v2

(Figure 1.E). As well, induction of recombinase DMC1 and Mos-kinase were revealed [10]. The strong dependence of ALT on the other two genes used for meiotic homology search Hop2-Mnd1 along with the directional telomere movement in all examined ALT cells was also earlier reported by Cho et al [17] hinting at the mutual mechanisms of ALT with meiotic prophase [18] for search and alignment of homologous chromosomes [19]. Assuming all this data and because the meiosis started by the recognition of the chromosome-specific subtelomere homologue sequences [20] particularly favoured by polyploidy [21], we suggested that meiotic recombination proteins and inverted meiosis, based on the pairing of subtelomeric sequences [20] may be involved in the repair of the damaged DNA in cancer ALT as schematized on Figure 1F. [10].

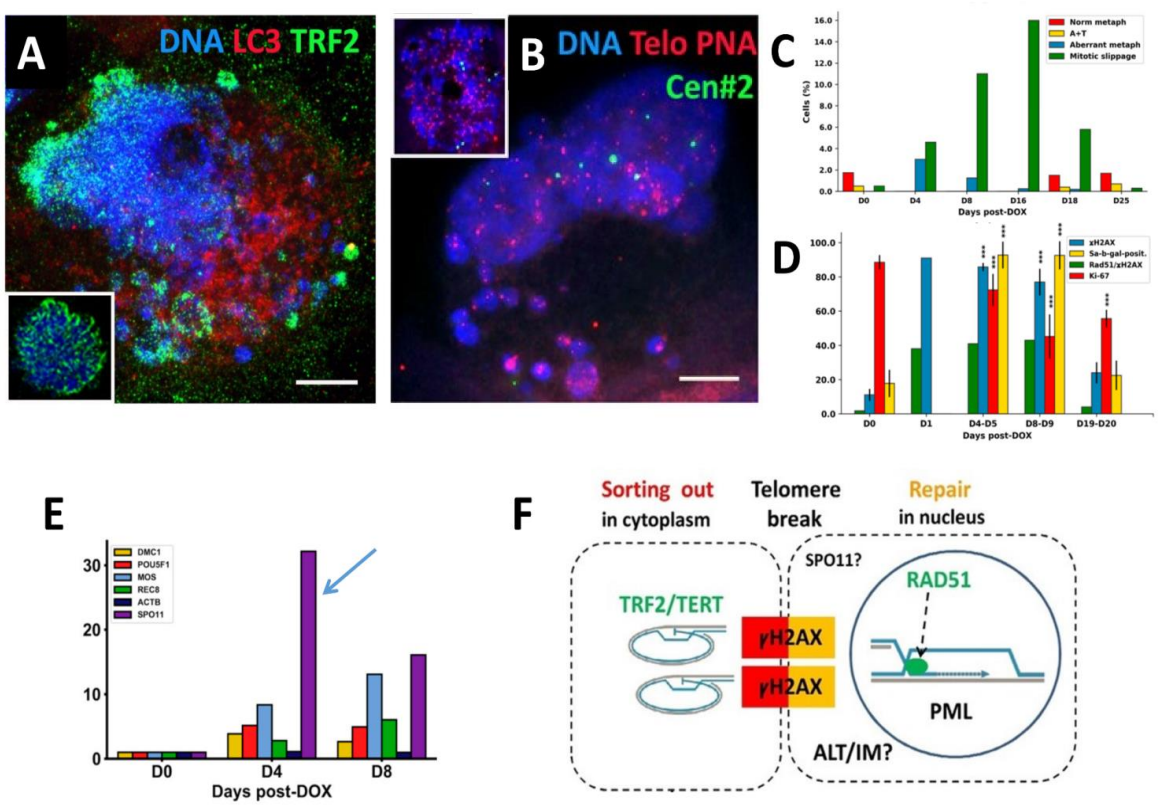

Figure 1. Alternative telomere lengthening (ALT) and repair by homologous recombination in PML bodies (APB) in the polyploidized MDA-MB-231 cells following DOX treatment. (A) Preferential release of the telomere shelterin-TRF2-associated chromatin into the cytoplasm (DOX-D7) (insert: normal metaphase of NT); (B) Fluorescence In Situ Hybridization (FISH) with the telomere and cen#2 probes showing retention of centromeres in the cell nucleus and release of a proportion of telomeres into the cytoplasm (DOX-D4) (insert: normal metaphase of NT); (C) representative differential mitotic counts of MDA-MB-231 cells following DOX treatment; (D) the dynamics of the senescence marker Sa-β-gal and proliferation marker Ki-67 along with DNA double-strand breaks (γH2AX) and their repair by homologous recombination—cells with colocalized Rad51/γH2AX foci. (ANOVA with post hoc analysis (Tukey's HSD test), *** $p < 0.001$. (E) Expression of the meiotic genes after DOX treatment, shown in folds; (F) A schematic showing the cytoplasmic sorting of hTERT/TRF2-marked DNA damage signalling telomere ends cut off by a telomere break during mitotic slippage. This process is associated with the ALT-RAD51-driven repair by homologous recombination of the two co-aligned trimmed telomeres occurring in specific nuclear PML (APB) bodies. ALT may be coupled with inverted meiosis (IM) by recombining homologous chromosomes conjugated by telomeres at the same breakage site possibly introduced by meiotic nuclease SPO11. Republished from [10] CC BY 4.0 licence.

 doi:10.20944/preprints202401.0111.v2

With these assumptions, we added to our immunofluorescence set, the antibodies for SPO11 and DMC1 (see Table in Methods). To generalise our findings, we performed experiments on this triple-negative breast cancer (MDA-DOX) and BRAF-CDk4-mutant melanoma cell line SkMel28 [22] (SkMel-DOX). Both used cell lines are also TP53 mutant, metastatic and aneuploid (para-triploid and para-tetraploid, correspondingly). We applied mild and sublethal concentrations of DOX-24-h treatment. As shown below in the Results, we could confirm the association of SPO11, as well as of RAD51 and DMC1 with APB after DOX-treatment of both cell lines, at the mild DOX100nM concentration. At sublethal DOX concentrations, we also found a formation of thread PML structures (apparently, PMLII isoform known for senescence [23,24] with affinity to the nuclear envelope [25] and characteristic of laminopathic progeria [26]). PML threads were particularly often seen in SkMel-DOX. We investigated by epifluorescent and confocal microscopy the topological relationship between telomere-enclosing thready PML structures in their dynamic interaction with lamin B1 in the progressively senescing cells and the capacity to repair DNA. The results, analysed together with the literature and own previous data on the lamin B1-associated the most peripheral chromatin layer (epichromatin) and its mobile derivatives – nuclear envelope limited chromatin sheets (ELCS) enriched in telomere sequences, ALU retrotransposons and PML, brought us to the hypothesis of the novel mechanism safeguarding the genome functionality by the concerted activity of PML and ELCS traffic with participation of meiotic proteins.

2. Materials and Methods

2.1. Cell Lines and Treatment

The triple-negative breast adenocarcinoma MDA-MB-231 cell line was obtained from the ECACC (European Collection of Authentic Cell Cultures, Wiltshire, UK). The human melanoma SK-MEL-28 cell line (mtB-RAF V600E, mtTP53) was obtained from the ATCC (The American Type Culture Collection, Manassas, VA, USA). Cells were cultured in flasks in Dulbecco's modified Eagle's media (DMEM) supplemented with 10% foetal bovine serum (FBS; Sigma-Aldrich, St. Louis, MO, USA) at 37 °C in a 5% CO2 humidified incubator without antibiotics. For experimental studies, cells were maintained in the log phase of growth and treated at 60-80% confluence with DOX (doxorubicin, D1515, Sigma-Aldrich, St. Louis, MO, USA) for 24 h at several concentrations (100, 250, 500, 1000 nM) for SK-MEL-28 cell line and 100nM for MDA-MB-231 cell line. After drug removal, cells were maintained by replenishing the culture medium every 2–3 days and sampled over 3 weeks post-treatment until the appearance of escape clones. In some experiments, cells were grown on chamber slides.

To determine growth kinetics, cells were seeded and treated with DOX at a density of 100,000 cells per well in a 6-well plate and counts were performed using a Neubauer camera (Heinz Herenz Medizinalbedarf GmbH Hamburg, Germany) and Trypan blue dye (0.4%) exclusion.

2.2. Immunofluorescence

Immunofluorescence staining was performed as described earlier [10]. Primary antibodies and their sources are listed in Table 1.

Table 1. The antibodies, their specificity, and their source.

Antibody against	Description	Specificity/Immunogen	Used concentration	Product no. and manufacturer
α-Tubulin	Mouse monoclonal	Recognizes an epitope located at the C-terminal end of the α-tubulin isoform in a variety of organisms	1:1000	T5168, Sigma-Aldrich, St. Louis, MO, USA

 doi:10.20944/preprints202401.0111.v2

DMC1	Rabbit polyclonal	Recombinant fragment corresponding to a region within amino acids 1 and 206 of DMC1	1:100	PA5-21472, Thermo fisher scientific, Waltham, MA, USA
γ-H2AX	Rabbit polyclonal	Recognizes mammalian, *yeast Drosophila melanogaster* and *Xenopus laevis* γ-H2AX	1:200	4411-PC-100, Trevigen, Gaithersburg, MD, USA
γ-H2AX	Mouse monoclonal	Synthetic peptide sequence surrounding phosphorylated Ser140	1:200	MA1-2022, Pierce, Waltham, MA, USA
LAMIN B1	Rabbit polyclonal	Peptide mapping at the C-terminus of Lamin B1 of human origin	1:200	ab1604, Abcam, Cambrige, UK
LC3	Rabbit polyclonal	The details of the immunogen for this antibody are not available	1:100	ab63817, Abcam, Cambrige, UK
MOS (C237)	Rabbit polyclonal	Epitope mapping at the C-terminus	1:50	sc-86, Santa Cruz, Dallas, TX, USA
PML	Rabbit polyclonal	A synthetic peptide corresponding to the N-terminus of the Human PML/RNF71/TRIM19	1:200	PA5-80910, Thermo fisher scientific, Waltham, MA, USA
PML	Mouse monoclonal	Epitope corresponding to amino acids 37-51 mapping near the N-terminal of PML of human origin	1:200	sc-966, Santa Cruz, Dallas, TX, USA
RAD51	Mouse monoclonal	Recombinant full length protein corresponding to Human Rad51 aa 1-338	1:50	ab213, Abcam, Cambrige, UK
SPO11	Mouse monoclonal	raised against amino acids 97-396 mapping at the C-terminus of Spo11 of human origin	1:50	sc-377161, Santa Cruz, Dallas, TX, USA
TRF2	Mouse monoclonal	His-tagged, fusion-protein, corresponding to full-length TRF2 (Telomeric Repeat binding Factor 2)	1:100	05-521, Millipore, Temecula, CA, USA

For microscopic observations, a fluorescence light microscope (Leitz Ergolux L03-10, Leica, Wetzlar, Germany) equipped with a colour video camera (Sony DXC 390P, Sony, Tokyo, Japan) and laser scanning confocal microscope (LEICA TCS SP8, Wetzlar, Germany) were used. To capture epifluorescence images, in addition to separate optical filters, a three-band BRG (blue, red, green) optical filter (Leica, Wetzlar, Germany) was applied.

2.3. Fluorescence in Situ Hybridization (FISH)

Telomere FISH for Telo PNA Cy3/Cen#2 FITC was performed with a peptide nucleic acid (PNA) telomere probe (Dako Inc., Glostrup, Denmark) in conjunction with a differentially coloured centromere 2 PNA probe (a gift from Dako, Inc., Glostrup, Denmark) as an internal reference point. FISH was applied following the procedure previously described [10,27].

 doi:10.20944/preprints202401.0111.v2

2.4. [3H]-thymidine autoradiography

DNA replicative activity in S-phase was determined in pulse experiments on irradiated (10 Gy) Namalwa lymphoma cell line by adding fresh [3H]-thymidine (Amersham) to a final concentration of 5 Ci/ml to the culture medium for 60 min. For more detail, see [28].

3. Results

3.1. The topological relationship of the components of ALT and lamin B1 in the time course post-DOX action. DNA repair and misrepair.

Non-treated breast cancer MDA MB 231 and melanoma SkMel28 cell lines in immunofluorescent staining of the used antibodies express some amount of meiotic recombination nuclease SPO11 and meiotic recombinase DMC1 particles, with affinity of SPO11 to mitotic telomeres; the cells are also Mos-kinase positive, particularly polyploid as earlier reported for these cell lines [10,29].

The spatial interactions between the marker of telomere end shelterin TRF2, PML body protein, γH2AX marker of DSBs, SPO11, RAD51, DMC1, and lamin B1 structures were examined by confocal microscopy in non-treated (NT) cells and after 24h-DOX treatment on days 4-9. In general, the topology and interaction of these nuclear components in response to DOX can be divided into five phases.

Phase I-II (juxta-position of ALT components).

Phase I: Co-parallel orientation of the long sparse arrays of the small PML-prebodies (0.2<1 μm), tiny TRF2 loci, and very small multiple SPO11 foci, with occasional colocalization, were seen in ~30-40 % of non-treated melanoma and breast cancer cells and in about 60-65% of DOX250 nM-treated cells on day 4-5 after 24h treatment; this pattern was more typical for multilobular polyploid nuclei (Figure 2A).

Phase II (Figure 2B insert and Figure 3): short arrays of more approached and increasingly colocalising components of maturing ALT-PML (APB) nuclear bodies (NB) were observed: PML, TRF2, γH2AX, SPO11 with RAD51 and also DMC1 recombinase (Figure 2B, boxed and Figure 3A-C). The arrays and clusters of telomere DNA sequence indirectly labelled by TRF2 were also confirmed by Telo-FISH (Figure 3D; for control, see insertion on Figure 1B).

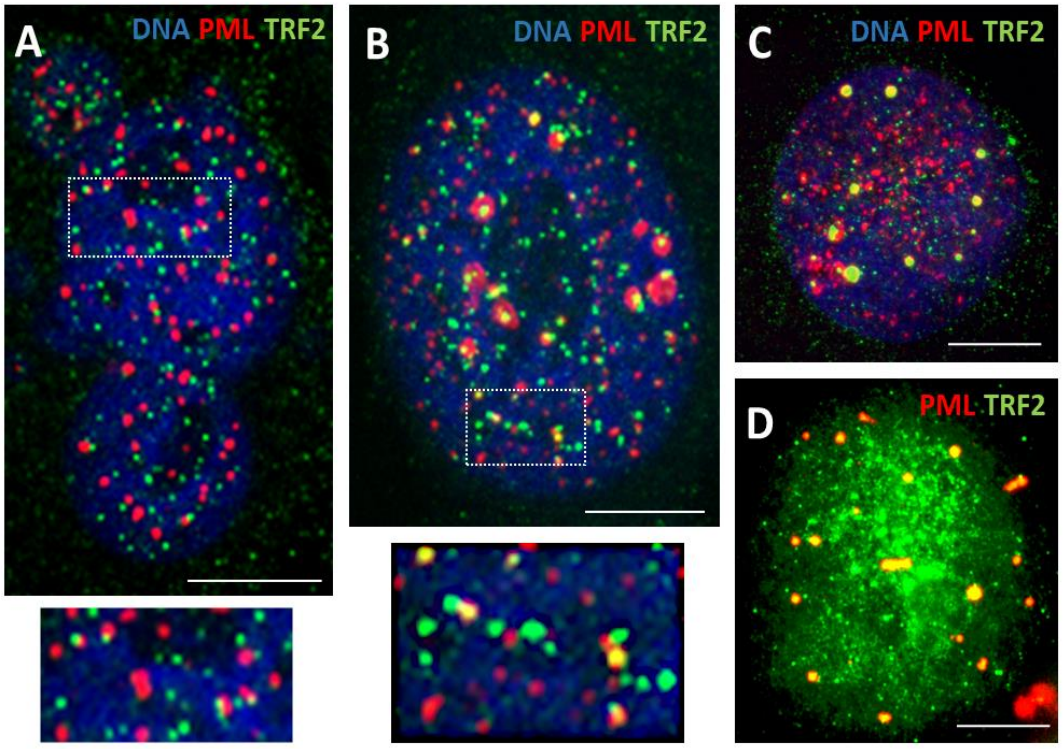

 doi:10.20944/preprints202401.0111.v2

Figure 2. Confocal images of the topology and interaction of ALT components - APB bodies and TRF2 in response to DOX. (A) SkMel28 cell showing co-parallel orientation of the long sparse arrays of the small PML-pre bodies (0.2<1 μm) and tiny TRF2 foci (DOX250nM-D5); (B) SkMel28 cell with mature ~ 1-2 μm round APB bodies including TRF2 foci; insert shows short arrays of more apposed and increasingly colocalising components of maturing APB nuclear bodies (DOX250nM-D5); (C) SkMel28 cell (DOX250nM-D5) and (D) MDA-MB-231 cell (DOX100nM-D7) both showing mature APB bodies colocalizing with TRF2 foci. Bars = 10 μm.

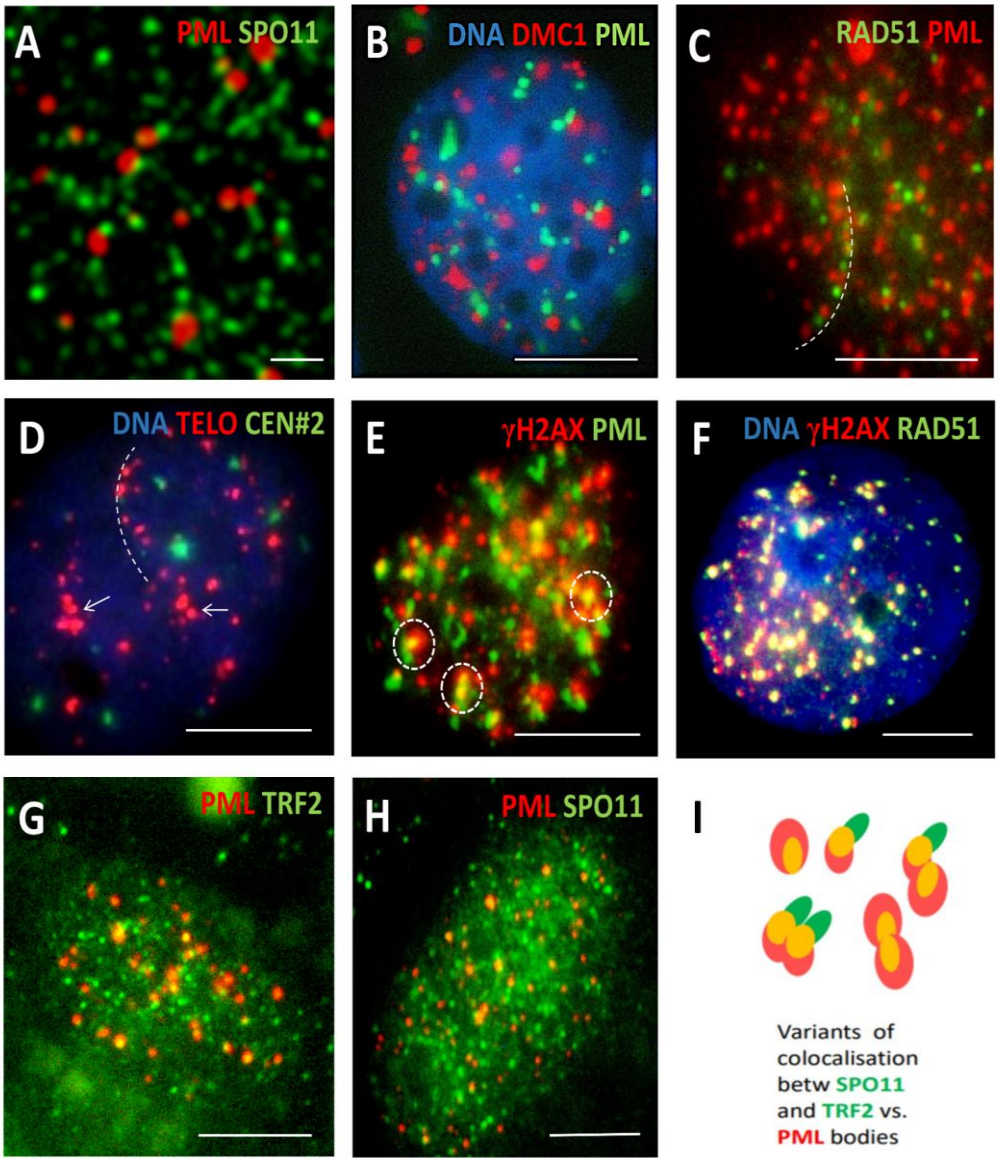

Figure 3. Interaction and colocalization of ALT components with maturing APB bodies in response to DOX. (A) Interaction of PML bodies with SPO11 foci in SkMel28 cell (DOX250nM-D5); (B) SkMel28 cell showing interaction of PML bodies with DMC1 recombinase (DOX250nM-D5); (C) Alignment of PML and RAD51 positive repair foci in SkMel28 cell (DOX250nM-D5); (D) Fluorescence In Situ Hybridization with the telomere and cen#2 probes showing arrays (dashed line) and clusters (arrows) of telomere DNA sequence in SkMel28 cell (DOX500nM-D5); (E) Formation of mature APB bodies including γH2AX foci in MDA-MB-231 cell (DOX100nM-D5); (F) Colocalization of γH2AX and RAD51 repair foci in MDA-MB-231 cell (DOX100nM-D5); (G) APB bodies including TRF2 foci in MDA-MB-231 cell (DOX100nM-D7); (H) MDA-MB-231 cell showing formation of mature APB bodies

 doi:10.20944/preprints202401.0111.v2

including SPO11 foci (DOX100nM-D7); (I) topological patterning of SPO11 and TRF2 foci with PML bodies. Bars: 1 μm for A, 10 μm for B-I.

3.1.2. Phase III (maturation of recombinogenic APBs)

Next, these short arrays formed mature ~ 1-2 μm round APB bodies including TRF2 foci, SPO11, γH2AX, RAD51 as found in 11-12% of cells (DOX 250 nM), mostly ~ 8C, on days 4-9 post-DOX (Figure 2B-D and Figure 3E-H). It was noted that the topological patterning of SPO11 and TRF2 foci with PML bodies, either in short arrays or colocalising in mature APB, were very similar, where PML bodies interacting with either of them was often seen in doublets, as schematised in Figure 3, I.

3.1.3. Phase IV: the formation of PML II isoform fibrillar structures

PML protein has seven isoforms, of them only one PMLII with a highly disordered Exon 7b forms the fibrillar structures as characteristic for senescing cells [25] and laminopathy progeria [26]. Here, PML fibrils constituting long ribbons were observed after sublethal doses 250 and 500nM DOX, more often in melanoma than MDA-DOX cells. It appears that the long PML tracks were formed by dimeric rods of PML NBs joined by TRF2-positive foci (Figure 4A). Concurrently, PML dimeric segments were dashed by yH2AX links (Figure 4B, small arrows), which could indicate to the non-homologous end-joining of DNA double-strand break-containing telomere repeats sticking in the PML tracks. These long strands of PML tended to form tangles converging to one knot (Figure 4A) and also rosettes around large clusters of yH2AX (Figure 4B, big arrows) or were seen as one or two concentric rings with small loops circumventing the nuclear periphery, supposing rotation around it (Figure 5A, B). Peripheral tracks of PML colocalized with the peripheral heterochromatin (Figure 5C, arrows); in addition, an inner network of PML tracks could also be seen in the continuity with peripheral threads. Their small loops containing fragments of lamin B1 (asterisk), sometimes were twisted in doublets (labelled by double asterisks). In these cells, lamin B1 was generally diffusely under-stained supposing its partial degradation (Figure 5C). Similarly, small loops in the concentric rings of Lamin B1 and of heterochromatin were revealed by us earlier in irradiated HeLa cells as described [10,30] and example in Figure 5D. The staining for a-tubulin and highly overexpressed MOS-kinase in the DOX-treated cells occasionally revealed concentric whorls of microtubules around nuclear envelope, interlaced with MOS, suggesting nuclear spinning by Mos-kinase phosphorylating the tubulin (Figure 5E). Mos is capable of organising a monopolar spindle for the meiotic bouquet rotation [10,31]. Moreover, to our surprise, we occasionally encountered in SkMel-DOX500 nM preparations, the tangled figure of PML threads interspersed by TRF2 foci reminding a telomere „bouquet" in meiotic zygotene (Figure 5F). The proteins of synaptonemal complexes (SCP1, SCP2, SCP3) were not studied here but are known to be expressed in cancers and melanoma; SCP3 was reported and previously seen in cancer cells at the nuclear envelope and cytoplasm [29,32].

Preprints.org (www.preprints.org) | NOT PEER-REVIEWED | Posted: 5 January 2024 doi:10.20944/preprints202401.0111.v2

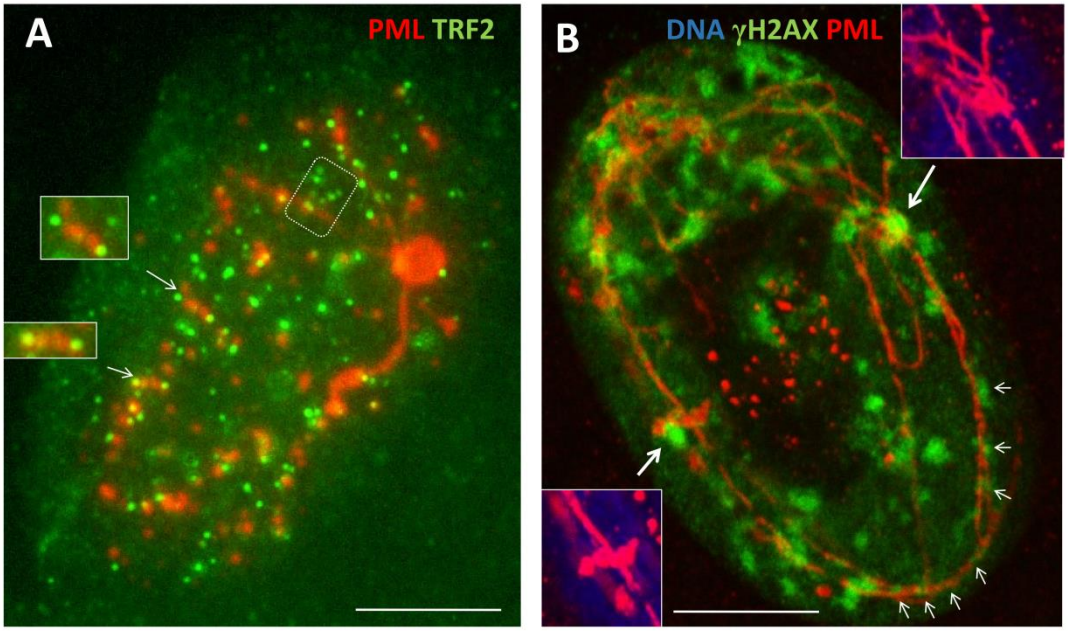

Figure 4. Formation of PMLII isoform fibrillar structures following DOX treatment. (A) SkMel28 cell showing long PML tracks by dimeric rods of PML NB joined by TRF2-positive foci (DOX500nM-D5); (B) PML dimeric segments dashed by yH2AX links (small arrows) in SkMel28 cell suggesting the non-homologous end-joining of DNA double-strand break-containing telomere repeats sticking in the PML tracks. Long strands of PML tend to form bows around large clusters of yH2AX (big arrows), (DOX250nM-D5). Bars = 10 μm.

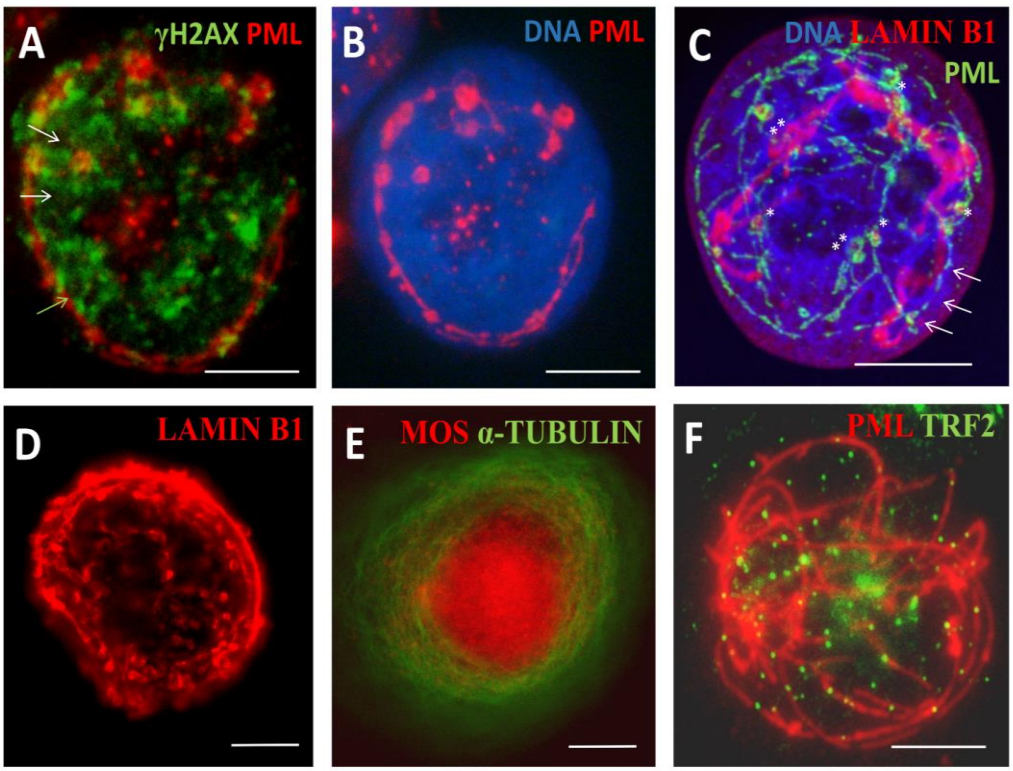

Figure 5. PML tracks and related structures spin around the cell nucleus. (A, B) SkMel28 with long PML fibrils seen as two concentric rings with small loops circumventing the nuclear periphery, supposing rotation around it (DOX250nM-D5); (C) Lamin B1 diffuse staining supposing its partial

 doi:10.20944/preprints202401.0111.v2

degradation, peripheral tracks of PML colocalized with the peripheral heterochromatin (arrows), small PML loops containing fragments of Lamin B1 (asterisk), sometimes were twisted in doublets (labelled by double asterisks) in SkMel28 cell (DOX250nM-D5), confocal maximal projection; (D) small loops in the concentric rings of Lamin B1 revealed in irradiated HeLa cells; (E) concentric whorls of microtubules around the nuclear envelope, interlaced with hyper-stained MOS, suggesting nuclear spinning by Mos-kinase phosphorylation of tubulin in MDA-MB-231 cell (DOX100nM-D7); (F) PML threads interspersed by TRF2 foci reminding a telomere „bouquet" in meiotic zygotene in SkMel28 cell (DOX500nM-D5). Bars = 10 μm. Figure 5D reproduced from [30] with permission from Elsevier, licence Nr 5691480400495. 17/12/23.

3.1.4. Thready PML and DNA recombination repair in DOX-treated cells

We wondered if and how thready PML were involved in the recombinative repair of the DNA damage. The counts of cells containing striped structures of PML for the presence of RAD51 foci after using DOX for both cell lines in comparison with cells displaying the APB foci are presented on Figure 6A. They showed that proportion of such Rad51-positive cells with striped PML structures was much lower than the proportion of RAD51-positive cells with typical small and large APB-bodies, still melanoma cells were relatively proficient in that and at 250-500 nM DOX concentrations still survived the damage (Figure 6B). As to the topology of the RAD51 foci in relation to the PML striped in these rare cells, Rad 51 is seen juxta-posed-colocalized with these structures but at the same time the pattern is chaotic (Figure 6C). In some cases, we could find the intermediate states between short tandem arrays of RAD51 foci, rarely colocalized with PML pre-bodies in continuation with short thread-like PML casually colocalized with small foci of RAD51 (Figure 6D), such indefinite patterns were occasionally seen in MDA-DOX. This observation may indicate that the state of short chains in preparation for telomere repair in APB is unstable and may as well not reach its goal - to form recombinative mature APB but turn to the formation of thready PML structures employing NHEJ which might acquire the affinity to lamin B1 starting rotation around nuclear periphery. The factors limiting recombinative maturation of APB in them may be due to the lack of SP-100 and SUMO reported for PML II thready isoform [25]. The rotation of PML/telomere threads around cell nuclei, indirectly observed as presented in Figure 5, can end in stage V, at the brink of cell death.

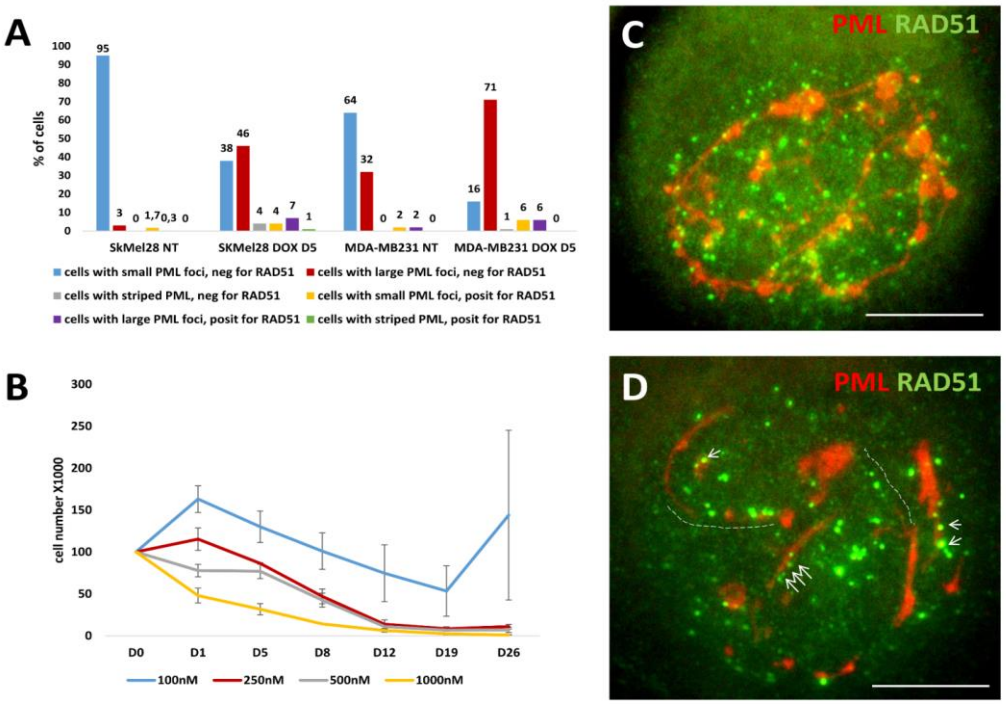

Figure 6. Cell growth and striped PML as related to Rad51-labelled DNA recombination repair after DOX. (A) The counts of cells containing small, large and striped structures of PML for the presence

 doi:10.20944/preprints202401.0111.v2

of RAD51 foci after DOX treatment (250 nM for SkMel28 and 100nM for MDA-MB-231 cells); (B) The SK-Mel28 cell growth curves for three independent experiments after DOX treatment (with SE); (C) Striped PML structures with RAD51 foci in SkMel28 cell (DOX250nM-D5); (D) short tandem arrays of RAD51 foci (dashed line), rarely colocalized with PML pre-bodies in continuation with short thready PML attracting small RAD51 foci (arrows) seen in SkMel28 cell (DOX250nM-D5). Bars on (C, D) = 10 μm.

3.1.5. Phase V, at the brink of catastrophe

In the transition from phase IV to V, with the low diffuse nuclear staining for lamin B1, we found both nucleus-circumventing PML tracks along with their segments dashed in large loops of lamin B1 suprastructures collapsing inside the nucleus (Figure A). In terminal cells, the lamin B1 thready suprastructures were formed tightly contorting within one or a few very large PML bodies, near or around nucleoli (Figure 7B). Less deeply senescent cells contain large yH2AX patches of unrepaired γH2AX /DNA surrounded or colocalized with the PML rosettes knotted near the intranucleolar invaginations of lamin B1 into the perinucleolar heterochromatin (Figure 4B, 7C, D). The lamin B1 folds invaginate towards multifacet PML structures around clusters of γH2AX formed within the perinucleolar (pericentric) chromatin and are also connected with PML tracks close to the nuclear envelope; these large PML bodies accumulate p62, a reporter of autophagic activity in this material as previously described [10].

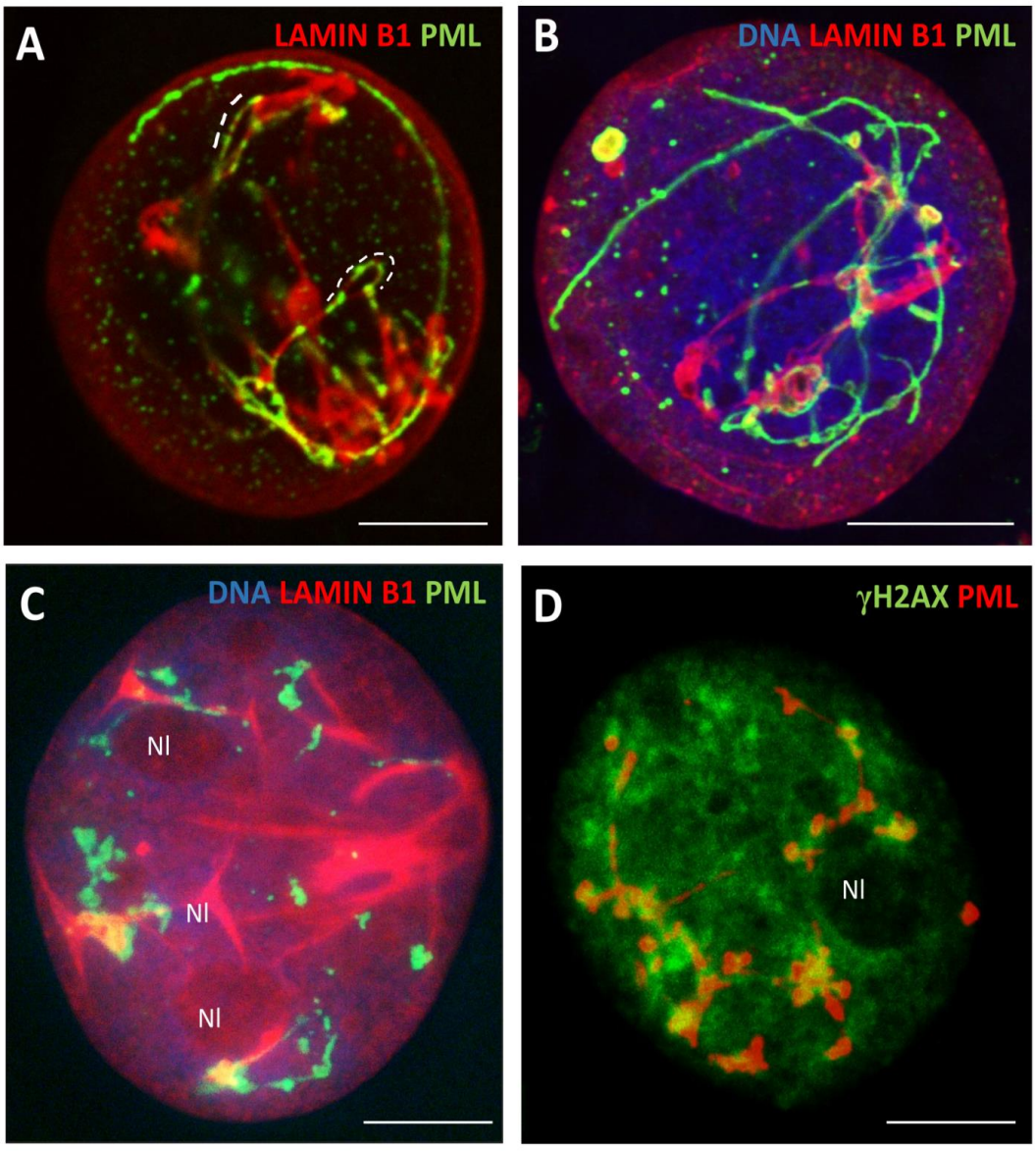

Preprints.org (www.preprints.org) | NOT PEER-REVIEWED | Posted: 5 January 2024 doi:10.20944/preprints202401.0111.v2

Figure 7. Topological relationships between the damaged DNA, PML, and lamin B1 structures in deeply senescent cells. (A) Lamin B1 is inserted into large loops of PML threads and PML rods intermit with Lamin B1 dashes (DOX250nM-D5); (B) the Lamin B1 thready structures formed within large PML bodies (DOX250nM-D5); (C-D) senescent cells contain large yH2AX patches of unrepaired γH2AX /DNA surrounded or colocalized with the PML near the intranucleolar invaginations of lamin B1 into the perinucleolar heterochromatin (DOX250nM-D5);(A-D) SkMel28 cells. Bars = 10 μm.

In general, our observations correspond to those published by Condemine et al [25,33] on the transfected isoforms of PML: "PML NBs assemble in "rosettes" surrounding DNA centromeres or are distributed in tracks bridging two centromeres". The APB PML enclose two telomere ends, while the giant PML NBs seen near nucleoli enclose satellite centromeric DNA [34]. Condemine [25] also mentions that PML "tracks can cross the nucleus and were frequently observed filing lamina gaps at the nuclear envelope". As well, our results are consistent with the recent paper applying superresolution microscopy showing that lamin B1 has a dashed character with γH2AX-clusters filling its gaps [35], coinciding with the earlier study by Olins showing the "partial colocalization of Lamin B1 and lamin B receptor (LBR) with the tendency of intermittent dashed pattern" [36,37].

The schematic, summarising our results on the topological relationship between PML-structures, ALT and nuclear lamin B1 is presented in Figure 8

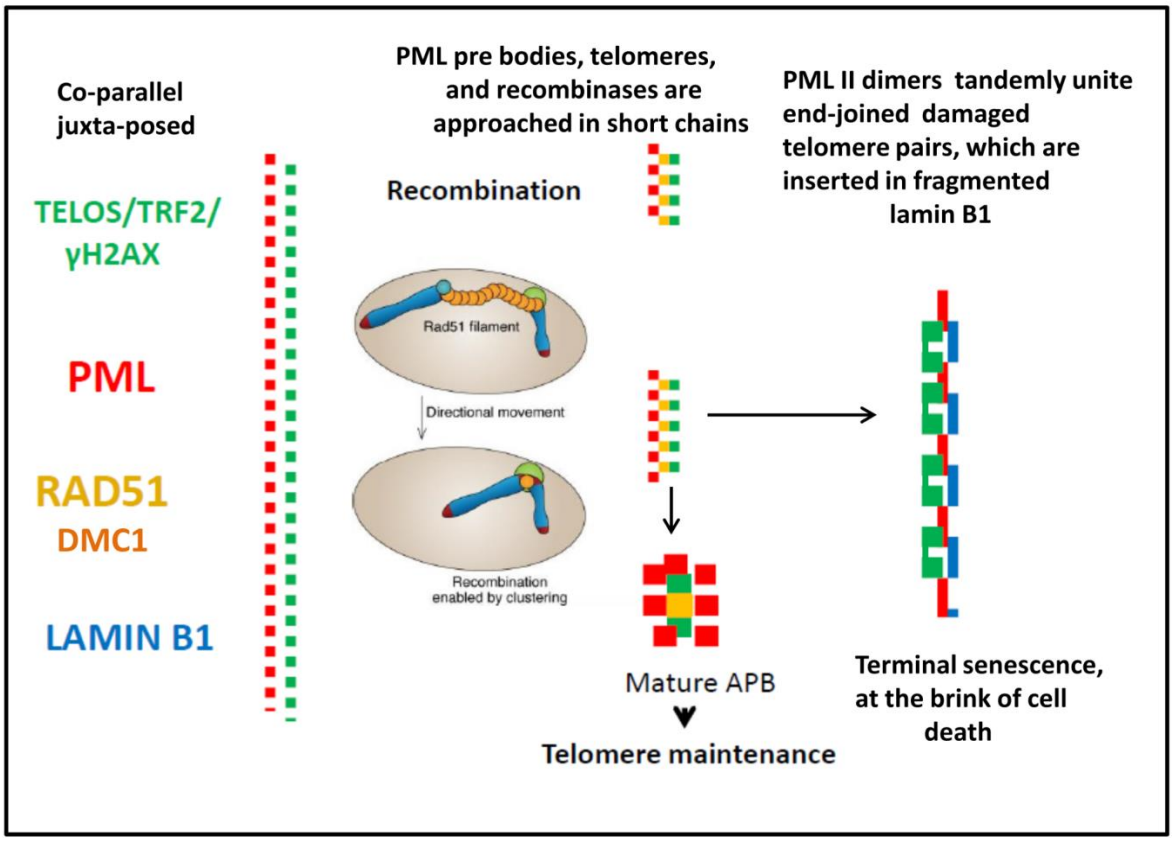

Figure 8. Schematic of the relationship between components of ALT and lamin B1 in the time course after DOX treatment depends on the result of the telomere repair. Conventional ALT supports telomere maintenance by recombination repair, while the telomeres that fail in ALT, likely undergo non-homologous end-joining supported by PML II fibrillar isoform dimers and can be inserted in fragmented lamin B1, to start nuclear rotation. The dashed, dynamic topology of the interacting substructures at all stages of the processes presumes its dissipative character.

The observed direct interaction of PML with lamin B1 and peripheral chromatin motivated us further to analyse their cooperation operating with the bulk literature related to the most peripheral heterochromatin and nuclear envelope-limited chromatin sheets (ELCS).

 doi:10.20944/preprints202401.0111.v2

3.2.1. The epichromatin and ELCS rotating around cell nuclei

So, we found the topological relationship of PML thready form associated with the damaged telomeres presumably coupled to the spinning mobility of the degrading nuclear lamin B1. Degradation of lamin B1 is occurring along with telomere attrition [3,38]. Lamin B1 and LBR embedded within the nuclear envelope, with the N-domain of the amphiphilic LBR interacting with heterochromatin, were shown as underlining the most peripheral and densely-packed 30-nm granules of "epichromatin" [36,37]. These DNAse-high salt-resistant chromatin granules were also coined "anchorosomes' ' by Fais et al [39]. Epichromatin forms flat folds - ELCS, lined by the inner and outer nuclear envelope [40]. They were first discovered by Davies [41] and seen in many animals and tissues. ELCSs are considered pathognomonic for leukaemia and many cancers as such [42]. Epichromatin and ELCS were extensively studied by Donald and Ada Olins in myeloid HL-60 cells differentiated by retinoic acids into multilobular neutrophils and also reviewed [37]. They revealed with collaborators more than 6,000 epichromatin fragments, ~1Kb average length, dispersed along all chromosomes, more densely at the telomeric ends [43], retaining canonical 30-nm chromatin structure, different from all other heterochromatin in cell nuclei [44].

In our EM and IF studies of the heavily γ-irradiated TP53 mutant lymphoma cell lines [45], we described the formation of ELCS correlating with induced polyploidy, nuclear segmentation and micronucleation enriched in the Ku70. The latter was shown by Celli et al [46] as promoting the non-homologous end-joining (NHEJ) of DNA breaks and the fusion of dysfunctional telomeres. In our study of irradiated p53 mutant lymphoma, we described the protrusions of heterochromatin into narrow folds of the nuclear envelope fusing two strands, from each nuclear side, with further separation and reunion of each strand with heterochromatin in another place of cell nucleus (as exampled on Figure 9A) [45]. In similar experiments on HeLa, we found the colocalization of lamin B1, peripheral heterochromatin and α-tubulin along the edges of the lobulating giant cell nuclei suggesting moving of these edges by microtubules (Figure 9 B-D), while in some experiments carried out on irradiated WI-L2-NS lymphoblastoma, the lobulating nuclear contours were found outlined by DMC1-recombinase (Figure 9E). The concentric rings of ELCS in the perinuclear space around nuclear lobes were beautifully demonstrated by A&D Olins [37] and reproduced with permission in Figure 9F, also undoubtedly indicating the nuclear lobulating mobility of ELCS. These images of fixed cells confirm the study of nuclear rotation on living cells by Paddock [47] showing that the interface of nuclear rotation is located either between the two nuclear membranes or in the adjacent cytoplasm.

 doi:10.20944/preprints202401.0111.v2

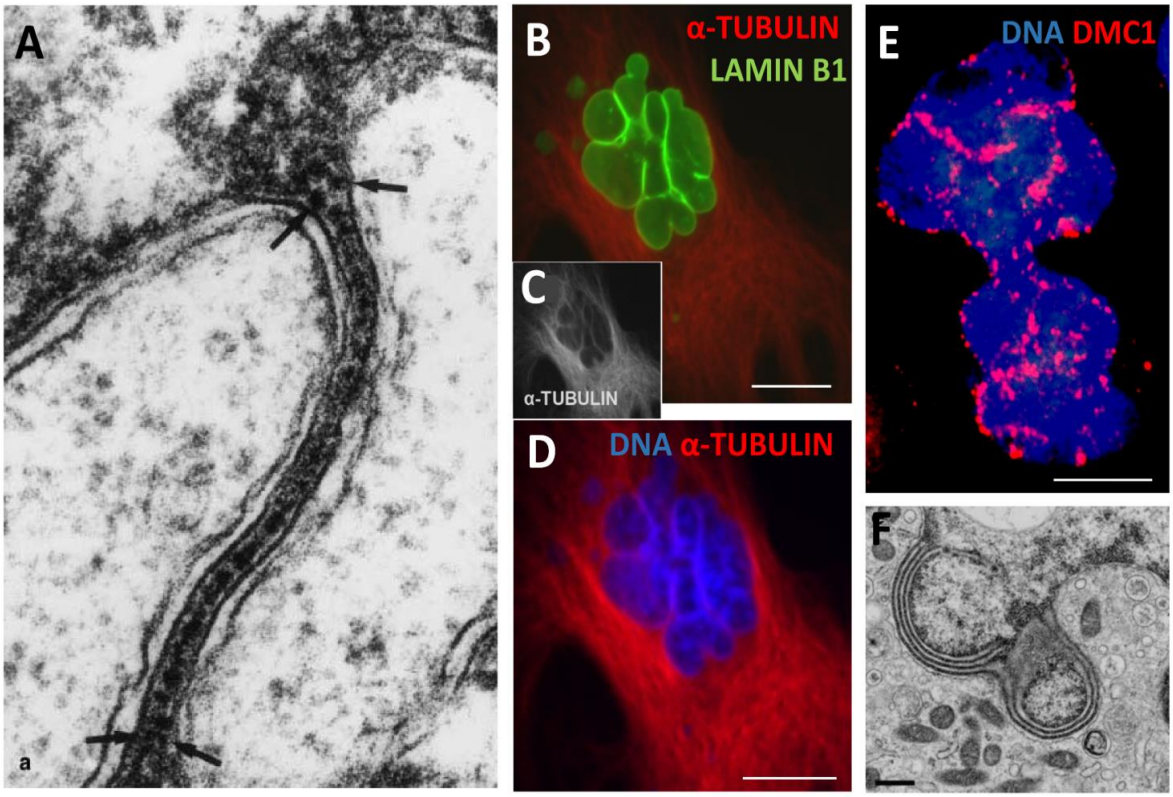

Figure 9. Nuclear envelope-limited lamin B containing chromatin sheets (ELCS) induced by genotoxic damage rotating around cell nuclei. (A) EM fragment of a Ramos lymphoma cell 7 days post 10 Gy irradiation showing protrusions of heterochromatin into narrow folds of the nuclear envelope fusing two strands, from each nuclear side, with further separation and reunion of each strand with heterochromatin in another place of cell nucleus (arrows); (B–D) colocalization of lamin B1, peripheral heterochromatin and α-tubulin along the edges of the lobulating large polyploid HeLa cell nucleus on day 5 post-10 Gy; (E) DMC1-recombinase outlines lobulating nuclear contours of WI-L2-NS lymphoblastoma cell 5 days post-5Gy; (F) The concentric rings of ELCS in the perinuclear space around nuclear lobes in HL-60 cell after retinoic acid treatment indicating mobility of ELCS. A republished from [45] with permission from Springer Nature, licence Nr 5693630419743, B-D republished from [30] with permission from Elsevier, licence Nr 5691480400495. 17/12/23; F - republished from [37], licence from Springer Nature order number 5692061501316.

Furthermore, in another study on intact MCF-7 breast cancer cells, we showed in situ by Acridine orange DNA structural test that differently from A-T-rich large lamin-associated domains (LADs) melting at 82^{0}C, the DNA of epichromatin is melting only at 94^{0}C suggesting that it is assuming a non-canonical hydrophobic DNA A-form revealed by R. Franklin and Gosling [48] along with the more hydrated canonical B-form. We suggested that due to this particular secondary DNA structure, the epichromatin can densely pack and favour the hydrophobic stacking of its supra nucleosome ~30 nm beads in the immediate hydrophobic microenvironment of the nuclear envelope [49]; a scheme of the epichromatin fragments assembly and relationship with LADs is reproduced on Figure 10.

 doi:10.20944/preprints202401.0111.v2

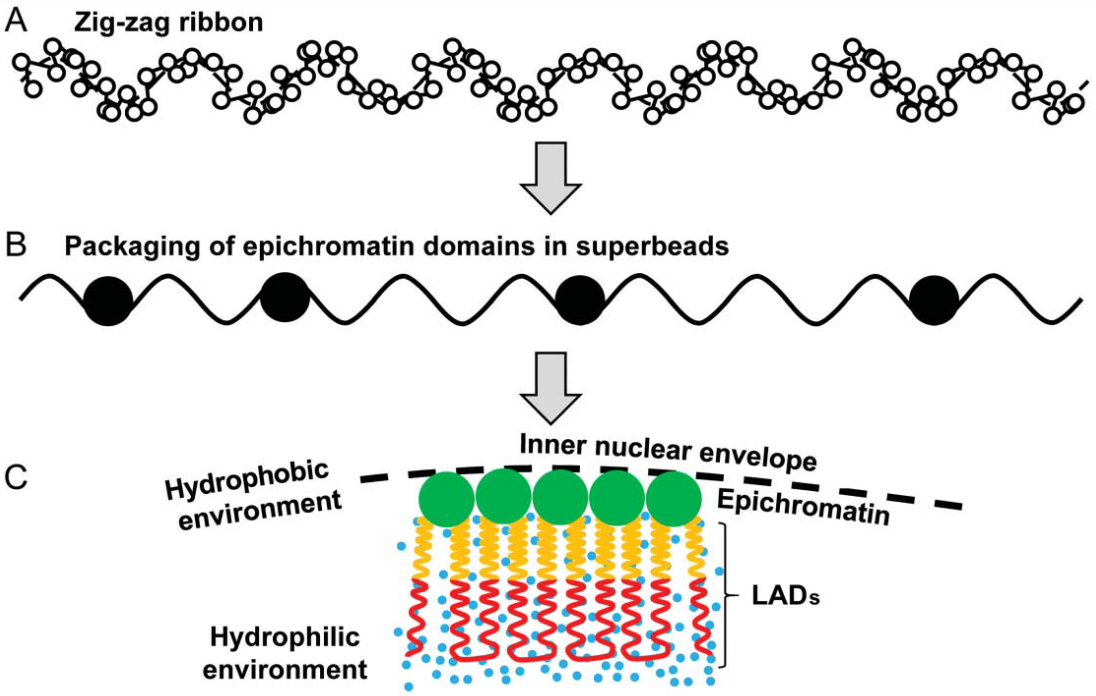

Figure 10. Schematics of the supra nucleosomal packaging and orientation of the epichromatin and inner LADs in the cell nucleus: (A) zig-zag ribbon of the di-nucleosomal units including ~ 6 nucleosomes per zig-zag pitch; (B) – packaging of epichromatin domains into super beads alternating with less densely packed segments of the inner LADs; (C) the intranuclear arrangement of epichromatin super beads under the nuclear envelope stacked by hydrophobic forces and repulsed from alternating, inner LADs, whose garlands are situated in the hydrophilic nuclear interior. The colours correspond to the range of AO staining in the DNA structural test. For simplicity, the relative size of the chromatin super beads on (C) is disproportionately enlarged. This figure is republished from [49] CC BY 4.0 licence.

Based on all these observations and the physical properties of the hard-packed epichromatin granules, we suggested that ELCS may be involved in the gear-wheel-like nuclear traffic for the chromosome homology search and rearrangements, enabling DNA repair or autophagic sorting, at the brink of survival [30,50,51]. Recently, Olins and colleagues, using cryo-EM demonstrated a criss-cross topology of the two epichromatin granular strands of ELCS [44] which well fits the supposed gear-wheel mechanism of the nuclear traffic of the two epichromatin globular strands in ELCSs.

D&A Olins worked out a monoclonal antibody HL2-6 for the epichromatin-specific histone-DNA epitope (H2A/H2B/DNA) which was also used by their methodology (double fixation) [52,53] in our lab confirming epichromatin as outlining telomeres in mitosis and underlining nuclear envelope as a thin rim in interphase described by the authors [49]. This antibody was used by Olins, Teif and colleagues for characterisation of epichromatin in chip-Seq studies.

3.2.2. Chip-Seq studies: Epichromatin meets PML and ALU

In chip-Seq studies of epichromatin domains in HL-60 cells, the important characteristics were described: the dominance of G-C over A-T sequences, GpC methylation, super-enrichment with ALU (S- and Y human) species - epichromatin encloses 30% of all nuclear ALU, while itself makes only 4-6% of the nuclear DNA [43,54], and high enrichment with PML proteins (18-fold) {53] shown in Figure 11A, B.

 doi:10.20944/preprints202401.0111.v2

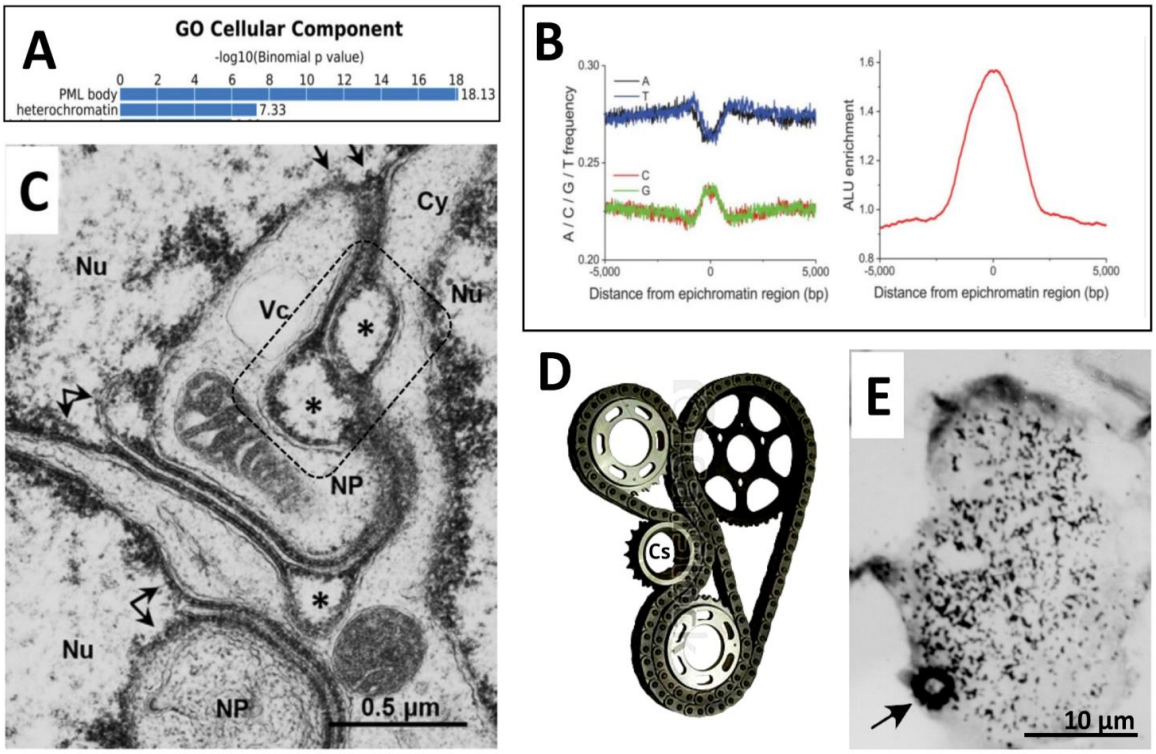

Figure 11. (A) Gene Ontology (GO) analysis of common epichromatin promoter regions, indicating that these domains are enriched in the heterochromatin genomic regions by the PML related proteins (top, a fragment); (B) Average feature distribution of common HL-60/S4 epichromatin regions as a function of the distance from the centre of these regions: enrichment of retrotransposon Alu repeats (right) and nucleotide frequencies (left); (C) EM fragment of a Namalwa lymphoma cell 7 days post 10 Gy irradiation showing the nuclear area enclosing the margins of three nuclear lobes. NU—nuclear lobes, NP—" nuclear pockets, Vc—vacuole; (D) The mechanical similarity of traffic of ELCS structures to gear-wheel principle; Cs - centrosome; (E) A gear-like chromatin structure (arrow) found in polyploid Namalwa cell, 10 Gy, D.8 by DNA radioautography, after the [3H-T] 60-min pulse. Figure 11A, B are republished from [54] by CC BY 4.0 licence; Figure 11C with permission from Elsevier, licence Nr 5691480400495. 17/12/23; Figure 11D reproduced from CSP 8924698, modified (insertion Cs).

3.2.3. ELCS are directly composed of telomere repeats

So, by Chip-Seq the epichromatin met with PML and ALU. Moreover, the study of ELCS in mouse brain stem B-cells with typical EM morphology described above, using FISH and IF revealed that the ELCS enclosed heterochromatin is consisting of telomere sequences (proved by Telo-FISH), tethered to lamin B1 by TRF2 [55]. This data do not contradict but, on the contrary, well fit with the affinity of the epichromatin conformation antibody to telomere ends clearly seen by IF in mitosis and in chip-Seq studies [43].

Summarising all this data, we have PML/ALT bodies in continuation with telomere-dashed fibrillar PML II form which interacts with lamin B1 and rotates in cell nuclei like mobile ELCS. This begins to look as a united, dynamic system. It remains to understand how this gear-wheel might be acting.

3.2.4. The traffic of ELCS structures from the analysis of EM pictures

A typical fragment of the thin section of irradiated multilobular Burkitt's lymphoma nucleus is reproduced in Figure 11C. This fragment showing the nuclear area enclosing the margins of three nuclear lobes (Nu) of a polyploid cell resembles a railway station junction (or a gear-wheel, see for the mechanical similarity Figure 11D) in a quite busy cell. At this site, the multiple ELCS on the upper

 doi:10.20944/preprints202401.0111.v2

nuclear lobe, powered by a large mitochondrion, protrude and split their double-strands, which pair with the single strand from another split ELCS or fuse with the heterochromatin from another site (shown with twig and double arrows) acting by the gear-wheel principle. In the bottom nuclear lobe, one strand of a splitted ELCS is forming a nuclear pocket (NP) with cytoplasmic content, such as earlier shown being involved in the local autophagy [45,51]. But in some places ELCSs typically form 'eyes', sized 0.3-0.5 μm, shortly disconnecting the two tightly apposed rows of epichromatin strands, this should certainly hamper this motion. Their function is unclear. However, we also see here the "double-eyes' (dash-boxed), which seems topologically allowing a crossover between four strands. Notably, in the immunoelectron study of the PMLII transfected form by [25], besides the lining nuclear envelope, the labelled bubbles of a similar size (~ 0.4 μm) found in the vicinity of the nuclear envelope were described. This similarity in size and location may suggest that PMLII is participating in the formation of these "eye" structures. Moreover, the observation presented in Figure 5A-C shows in our current SkMel-DOX250 experiment similar small PML-positive loops along the PML threads, sometimes as twisted doublets containing the fragments of lamin B1 (Figure 5C). Collectively, these observations suggest that ELCS and their derivatives composed of the epichromatin telomere sequences employ the PMLII isoform interacting with fragments of lamin B1 for the gear-wheel traffic. It is moved by the microtubules as clearly seen in Figure 9B-D, which should be driven from a centrosome (designed Cs on Figure 11D). Therefore, paradoxically, we found occasionally a typical gear-like heterochromatic structure of the densely pulse-labelled (60 min) DNA along with the dashed label of elongated chromatin threads (Figure 11E).

4. Discussion

4.1. The telomere repair and misrepair in accelerated cellular senescence (ACS)

Telomeres have a central role in chromosomal and nuclear stability events. On the other hand, free chromosome ends, dysfunctional telomeres, and interstitial telomeric sequences (ITS) can trigger chromosome rearrangements and are involved in evolutionary adaptations [56]. Accelerated cellular senescence (ACS) induced in TP53 mutant cancer cells by stress and anticancer drugs response also unites two opposite processes: it stops mitotic divisions by MS for one to three weeks but this interval accumulating stressed polyploid cells seems needed for proliferation to be further resumed in cell minority which rescue from DNA damage and provide resistant tumour growth. Besides telomere attrition and decrease of lamin B1, the ACS depth is characterized by progressive DNA demethylation, and activation of retrotransposons [57].

With interruption of mitotic division by MS, the halving of the semi-conservatively replicated chromosomes for the linear transfer of genetic material is also interrupted. We can consider as a hypothesis that this interruption is needed for DNA repair and cell survival by the mechanism, which is not associated with the linear transfer of genetic information. Then, what?

4.2. Telomeres, ALU flipons, and non-linear information transfer

For the alternative solution, we have four hints : (1) It is abundance of SPO11 meiotic nuclease in these NT and much more, in DOX-treated polyploid cancer cells (Figure 1E, Figure 3A, H); (2) the observation of SPO11 identical topology with telomeric shelterin TRF2 in relation to PML pre-bodies and mature NBs; (3) yet unexplained super-enrichment of the epichromatin composed of telomere sequences [55] with ALU-retrotransposons [43,54]; (4) our previous observations on the unscheduled DNA synthesis moving the 90-min selectively BrdU-labelled material from perinucleolar rim to ELCS loops together with fibrillarin, in the embryonal carcinoma induced ASCs which can be interpreted as the involvement of activated retrotransposons in the nuclear traffic [30].

The meiotic recombinative nuclease SPO11 is rather peculiar. Boateng et al [58] showed in mice that significant homolog pairing needs SPO11 (and SUN1 of the nuclear envelope) and is occurring still before the programmed meiotic DNA cleavage by SPO11. Moreover, SPO11 initiates DNA DSB not in random sites and maybe, not only in conventional meiosis. Recent studies showed that SPO11 prefers to cut sequences with similarity to a DNA-bending motif. Double DSB signals induced by

 doi:10.20944/preprints202401.0111.v2

SPO11 overlap and correlate with topoisomerase II-binding sites, which points to a role for topological stress and DNA crossings in break formation and suggests a model for the formation of DSBs and double DSBs in which Spo11 traps two DNA strands. Double DSB gaps, formed by SPO11 which make up an estimated 20% of all initiation events, can account for full non-Mendelian gene conversion events [59] which is favoured by polyploidy [60]. The core meiotic genes including those revealed in our study in cancer ALT are also active in the asexual Entamoeba (Spo11, Hop1, Hop2, Mnd1, Mlh1, Mlh2, Pms1, Dmc1, Msh2, Msh4, Msh5, Msh6, Rad50, Rad51 and Rad52) suggesting the possible ancestral traits in human genome [61].

Compared to other mammals, the genomes of primates and particularly humans are enriched with large, interspersed segmental duplications (SDs), repeated in two or more genomic locations, with high levels of sequence identity. These duplications show clustering and up to 10-fold enrichment within pericentromeric and subtelomeric regions [59,62].

Detailed analyses of the sequences of pairwise SD alignments have revealed that SINE/AlU, the most abundant RT class of mobile elements, is significantly enriched at the boundaries of SD pairs and restricted to younger subfamilies (AluY and AluS). The pairwise SD boundaries were shown to be fragile and the preferential sites of double-strand breakage. The fragile human genome sites assume a left-handed zigzag-like Z-DNA form of high energy tension and represent the loci of the high mutation and deletion rates [63]. In particular, interstitial inverted telomere duplications in the mammalian genome are flanked by the fragile ALU sequences [64] typically assuming the DNA structure of so-called Z-flipons [65].

So, SPO11 is affine to and eager of cutting through ALU sequences flanking telomere repeats. Shelterin TRF1 controls common fragile sites containing interstitial telomere repeats [66] and attracts TRF2 and also, potentially PML as schematized in (Figure 12).

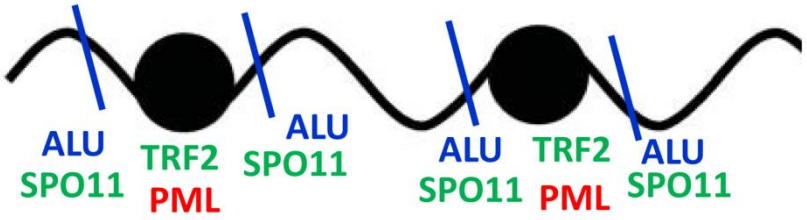

Figure 12. Potential sites of ALT along the length of chromosome DNA composed of end- or interstitial telomeres shown as dense epichromatin balls (the inverted repeats and clusters are not shown for simplicity), affine for TRF2 and PML, flanked by ALU fragile Z-DNA sites with the affinity for SPO11 capable to cut through these torsionally stressed DNA fragments (blue lines). This situation is corresponding to Phase I of the coparallel juxta-position of the potential components of ALT predisposing to Phase II of short chains (as shown in Figure 2A, B and schematically in Figure 8).

These potential actors of ALT juxta-pose along the chromosomes to epichromatin telomere domains and can become mobile by SPO11 cuts through ALU-Z-DNA (occurring, possibly, in replicative stress of polyploidisation) as molecular ensambles, find a pair, attract RAD51, and repair the telomere damage by recombination in mature APBs. The mechanism may be similar to inverted meiosis recombining on subtelomeres [10]. The direct participation of DMC1 in ALT remains unclear. Alternatively, the unrepaired by HR telomere pairs stack into PMLII tracts by NHEJ. This process occurring with active involvements of the potentially mobile ALU-Z flipons is orthogonal to linear transfer of genetic information in conventional cell cycle, which is interrupted (with purpose?) by ACS. By the model of Alan Herbert [65], the flipons (the sites of non-conventional DNA conformations) serve as dissipative structures for binary switches. They expand the repertoire of RNAs compiled from an involved gene. Their action greatly increases the informational capacity of linearly encoded genomes. Likely, just this process is involved in the described events associated with

 doi:10.20944/preprints202401.0111.v2

ASC involving telomeres, PML in NBs and thread isoforms, ALU and the lamin B1-lined two-stranded mobile ELCS enclosing them. It is not excluded that the ELCS traffic using the resource from autophagy of sorted micronuclei and ELCS nuclear pockets may return cancers from the brink of cell death [30,51,67].

4.3. ELCS nuclear traffic and chromothripsis

Several points indicate that the discussed issue associating telomere surveillance with the proposed mechanism of the gear-wheel ELCS traffic interacting with a PML isoform system may be related to the karyotype restructuring by chromothripsis (chromoanagenesis). Below, to be short, we just compile the literature data and, highlight in bold the key words which are consistent with this idea.

Chromothripsis events characterised by massive, c**lustered genomic rearrangements** pervasive across 46% of patient **cancers** have a link with **telomere damage** and cancer **hyperploidy** [68,69], and it may be reversible [70]. This punctuated karyotype evolution represents a powerful survival strategy for somatic cells under high levels of **stress/selection** [71]. Chromothripsis uses non-homologous **end-joinin**g, shaping the genomic landscape [70,72]. It is an adaptive survival tool of **macroevolution** [73].

5. Conclusions

The XXI century started the era of New Biology, dealing with the complexity and the latest evolution of the mammalians and humans [74]. The attempts of most researchers in the XX century to understand cancer with the rules and means of basic molecular biology largely failed [74,75]. However, the tremendous efforts to win against cancer began to paradoxically reveal the Biology of Complexity itself as dealing with dissipative adaptive Systems [76]. While the Weisman's and Mendelian inheritance laws keep us to the conventional mitosis, meiosis and recombination between homologues, the presence of jumping transposable elements discovered by [77] comprising nearly half of human DNA, segmental duplications, including interstitial telomeres, and the disordered proteins indicate the existence of non-linear regulation and transfer of genetic information in addition to the linear one, allowing survival of complex systems. The story of the two telomere repair pathways in cancer, occurring with shifting between PML isoforms showing the adaptive switch between two pathways – the error-free HR in APBs/PML I and the error-prone NHEJ aided by PML II and lamin B1, performed during accelerated cell senescence and still compatible with survival, just reflects this duality in regulation of complex systems. It appears that meiotic nuclease SPO11 is starting both pathways. We hope that our observations and the hypothesis of the gear-wheel nuclear traffic will stimulate further research.

Author Contributions: "Conceptualization, J.E. and K.S.; methodology, validation, K.S. and F.R.; formal analysis, X.X.; investigation, K.S., J.E., F.R., D.P..; resources, K.S., D.P..; writing—original draft preparation, J.E. and K.S.; writing—review and editing, J.E., D.P.; visualization, K.S., J.E.; supervision, J.E.; project administration, K.S.; funding acquisition, K.S All authors have read and agreed to the published version of the manuscript.

Funding: This research was funded by a Fundamental and Applied Research Project lzp-2022/1-0114. The publication was supported by the International Visegrad Fund through Visegrad Grants within the project "Inclusion of Young Researchers from the V4 Region in Top Research on the Cell Nucleus" (project ID 22230207).

Institutional Review Board Statement: Not applicable.

Informed Consent Statement: Not applicable.

Acknowledgments: We thank Harry Scherthan, Munich, Germany, for support with telomere FISH probes. Pawel Zayakin is greatly acknowledged for his interest and formatting of the paper.

Conflicts of Interest: The authors declare no conflict of interest.

 doi:10.20944/preprints202401.0111.v2

Abbreviations

ACS - Accelerated cell senescence; ALT- alternative telomere lengthening; APBs - ALT-associated PML bodies; DOX - doxorubicin; ELCS - nuclear envelope limited chromatin sheets; FISH - In Situ Hybridization; IM - inverted meiosis; ITS - interstitial telomeric sequences; MS - mitotic slippage; NHEJ - non-homologous end-joining; Nu - nuclear lobes; NP - nuclear pocket; LADs - lamin-associated domains; LBR - lamin B receptor; PML NBs - the promyelocytic leukaemia nuclear bodies; SDs - segmental duplications; TERT - Telomerase reverse transcriptase; TRF2 - Telomeric repeat-binding factor 2

References

1. Roninson, I.B.; Broude, E.V.; Chang, B.D. If Not Apoptosis, Then What? Treatment-Induced Senescence and Mitotic Catastrophe in Tumor Cells. *Drug Resist. Updat.* **2001**, *4*, 303–313.
2. Victorelli, S.; Passos, J.F. Telomeres and Cell Senescence - Size Matters Not. *EBioMedicine* **2017**, *21*, 14–20.
3. Shay, J.W. Telomeres and Aging. *Curr. Opin. Cell Biol.* **2018**, *52*, 1–7.
4. Freund, A.; Laberge, R.-M.; Demaria, M.; Campisi, J. Lamin B1 Loss Is a Senescence-Associated Biomarker. *Mol. Biol. Cell* **2012**, *23*, 2066–2075.
5. Ivanov, A.; Pawlikowski, J.; Manoharan, I.; van Tuyn, J.; Nelson, D.M.; Rai, T.S.; Shah, P.P.; Hewitt, G.; Korolchuk, V.I.; Passos, J.F.; et al. Lysosome-Mediated Processing of Chromatin in Senescence. *J. Cell Biol.* **2013**, *202*, 129–143.
6. Campisi, J. Aging, Cellular Senescence, and Cancer. *Annu. Rev. Physiol.* **2013**, *75*, 685–705.
7. De Cecco, M.; Criscione, S.W.; Peckham, E.J.; Hillenmeyer, S.; Hamm, E.A.; Manivannan, J.; Peterson, A.L.; Kreiling, J.A.; Neretti, N.; Sedivy, J.M. Genomes of Replicatively Senescent Cells Undergo Global Epigenetic Changes Leading to Gene Silencing and Activation of Transposable Elements. *Aging Cell* **2013**, *12*, 247–256.
8. Puig, P.-E.; Guilly, M.-N.; Bouchot, A.; Droin, N.; Cathelin, D.; Bouyer, F.; Favier, L.; Ghiringhelli, F.; Kroemer, G.; Solary, E.; et al. Tumor Cells Can Escape DNA-Damaging Cisplatin through DNA Endoreduplication and Reversible Polyploidy. *Cell Biol. Int.* **2008**, *32*, 1031–1043.
9. Lezaja, A.; Altmeyer, M. Dealing with DNA Lesions: When One Cell Cycle Is Not Enough. *Curr. Opin. Cell Biol.* **2021**, *70*, 27–36.
10. Salmina, K.; Bojko, A.; Inashkina, I.; Staniak, K.; Dudkowska, M.; Podlesniy, P.; Rumnieks, F.; Vainshelbaum, N.M.; Pjanova, D.; Sikora, E.; et al. "Mitotic Slippage" and Extranuclear DNA in Cancer Chemoresistance: A Focus on Telomeres. *Int. J. Mol. Sci.* **2020**, *21*, doi:10.3390/ijms21082779.
11. Mosteiro, L.; Pantoja, C.; Alcazar, N.; Marión, R.M.; Chondronasiou, D.; Rovira, M.; Fernandez-Marcos, P.J.; Muñoz-Martin, M.; Blanco-Aparicio, C.; Pastor, J.; et al. Tissue Damage and Senescence Provide Critical Signals for Cellular Reprogramming in Vivo. *Science* **2016**, *354*, doi:10.1126/science.aaf4445.
12. Milanovic, M.; Fan, D.N.Y.; Belenki, D.; Däbritz, J.H.M.; Zhao, Z.; Yu, Y.; Dörr, J.R.; Dimitrova, L.; Lenze, D.; Monteiro Barbosa, I.A.; et al. Senescence-Associated Reprogramming Promotes Cancer Stemness. *Nature* **2018**, *553*, 96–100.
13. Jackson, T.R.; Salmina, K.; Huna, A.; Inashkina, I.; Jankevics, E.; Riekstina, U.; Kalnina, Z.; Ivanov, A.; Townsend, P.A.; Cragg, M.S.; et al. DNA Damage Causes TP53-Dependent Coupling of Self-Renewal and Senescence Pathways in Embryonal Carcinoma Cells. *Cell Cycle* **2013**, *12*, 430–441.
14. Huna, A.; Salmina, K.; Erenpreisa, J.; Vazquez-Martin, A.; Krigerts, J.; Inashkina, I.; Gerashchenko, B.I.; Townsend, P.A.; Cragg, M.S.; Jackson, T.R. Role of Stress-Activated OCT4A in the Cell Fate Decisions of Embryonal Carcinoma Cells Treated with Etoposide. *Cell Cycle* **2015**, *14*, 2969–2984.
15. Erenpreisa, J.; Salmina, K.; Anatskaya, O.; Cragg, M.S. Paradoxes of Cancer: Survival at the Brink. *Semin. Cancer Biol.* **2022**, *81*, 119–131.
16. Jafri, M.A.; Ansari, S.A.; Alqahtani, M.H.; Shay, J.W. Roles of Telomeres and Telomerase in Cancer, and Advances in Telomerase-Targeted Therapies. *Genome Med.* **2016**, *8*, 69.
17. Cho, N.W.; Dilley, R.L.; Lampson, M.A.; Greenberg, R.A. Interchromosomal Homology Searches Drive Directional ALT Telomere Movement and Synapsis. *Cell* **2014**, *159*, 108–121.
18. Arnoult, N.; Karlseder, J. ALT Telomeres Borrow from Meiosis to Get Moving. *Cell* 2014, *159*, 11–12.
19. Burla, R.; La Torre, M.; Saggio, I. Mammalian Telomeres and Their Partnership with Lamins. *Nucleus* **2016**, *7*, 187–202.
20. Calderón, M. del C.; Rey, M.-D.; Cabrera, A.; Prieto, P. The Subtelomeric Region Is Important for Chromosome Recognition and Pairing during Meiosis. *Sci. Rep.* **2014**, *4*, 6488.
21. Aguilar, M.; Prieto, P. Telomeres and Subtelomeres Dynamics in the Context of Early Chromosome Interactions During Meiosis and Their Implications in Plant Breeding. *Front. Plant Sci.* **2021**, *12*, 672489.

22. Smalley, K.S.M.; Lioni, M.; Dalla Palma, M.; Xiao, M.; Desai, B.; Egyhazi, S.; Hansson, J.; Wu, H.; King, A.J.; Van Belle, P.; et al. Increased Cyclin D1 Expression Can Mediate BRAF Inhibitor Resistance in BRAF V600E-Mutated Melanomas. *Mol. Cancer Ther.* **2008**, *7*, 2876–2883.
23. Jensen, K.; Shiels, C.; Freemont, P.S. PML Protein Isoforms and the RBCC/TRIM Motif. *Oncogene* **2001**, *20*, 7223–7233.
24. Nisole, S.; Maroui, M.A.; Mascle, X.H.; Aubry, M.; Chelbi-Alix, M.K. Differential Roles of PML Isoforms. *Front. Oncol.* **2013**, *3*, 125.
25. Condemine, W.; Takahashi, Y.; Zhu, J.; Puvion-Dutilleul, F.; Guegan, S.; Janin, A.; de Thé, H. Characterization of Endogenous Human Promyelocytic Leukemia Isoforms. *Cancer Res.* **2006**, *66*, 6192–6198.
26. Wang, M.; Wang, L.; Qian, M.; Tang, X.; Liu, Z.; Lai, Y.; Ao, Y.; Huang, Y.; Meng, Y.; Shi, L.; et al. PML2-Mediated Thread-like Nuclear Bodies Mark Late Senescence in Hutchinson-Gilford Progeria Syndrome. *Aging Cell* **2020**, *19*, e13147.
27. Scherthan, H.; Sotnik, N.; Peper, M.; Schrock, G.; Azizova, T.; Abend, M. Telomere Length in Aged Mayak PA Nuclear Workers Chronically Exposed to Internal Alpha and External Gamma Radiation. *Radiat. Res.* **2016**, *185*, 658–667.
28. Illidge, T.M.; Cragg, M.S.; Fringes, B.; Olive, P.; Erenpreisa, J.A. Polyploid Giant Cells Provide a Survival Mechanism for p53 Mutant Cells after DNA Damage. *Cell Biol. Int.* **2000**, *24*, 621–633.
29. Pjanova, D.; M. Vainshelbaum, N.; Salmina, K.; Erenpreisa, J. The Role of the Meiotic Component in Reproduction of B-RAF-Mutated Melanoma: A Review and "brainstorming" Session. In *Melanoma*; IntechOpen, 2021 ISBN 9781838808785.
30. Erenpreisa, J.; Salmiņa, K.; Belyayev, A.; Inashkina, I.; Cragg, M.S. Survival at the Brink. In *Autophagy: Cancer, Other Pathologies, Inflammation, Immunity, Infection, and Aging*; Elsevier, 2017; pp. 275–294 ISBN 9780128121467.
31. Verlhac, M.H.; Kubiak, J.Z.; Weber, M.; Géraud, G.; Colledge, W.H.; Evans, M.J.; Maro, B. Mos Is Required for MAP Kinase Activation and Is Involved in Microtubule Organization during Meiotic Maturation in the Mouse. *Development* **1996**, *122*, 815–822.
32. Salmina, K.; Huna, A.; Kalejs, M.; Pjanova, D.; Scherthan, H.; Cragg, M.S.; Erenpreisa, J. The Cancer Aneuploidy Paradox: In the Light of Evolution. *Genes* **2019**, *10*, doi:10.3390/genes10020083.
33. Condemine, W.; Takahashi, Y.; Le Bras, M.; de Thé, H. A Nucleolar Targeting Signal in PML-I Addresses PML to Nucleolar Caps in Stressed or Senescent Cells. *J. Cell Sci.* **2007**, *120*, 3219–3227.
34. Corpet, A.; Kleijwegt, C.; Roubille, S.; Juillard, F.; Jacquet, K.; Texier, P.; Lomonte, P. PML Nuclear Bodies and Chromatin Dynamics: Catch Me If You Can! *Nucleic Acids Res.* **2020**, *48*, 11890–11912.
35. Chapman, K.B.; Filipsky, F.; Peschke, N.; Gelléri, M.; Weinhardt, V.; Braun, A.; Hausmann, M.; Cremer, C. A Comprehensive Method to Study the DNA's Association with Lamin and Chromatin Compaction in Intact Cell Nuclei at Super Resolution. *Nanoscale* **2023**, *15*, 742–756.
36. Olins, A.L.; Rhodes, G.; Welch, D.B.M.; Zwerger, M.; Olins, D.E. Lamin B Receptor: Multi-Tasking at the Nuclear Envelope. *Nucleus* **2010**, *1*, 53–70.
37. Olins, D.E.; Olins, A.L. Nuclear Envelope-Limited Chromatin Sheets (ELCS) and Heterochromatin Higher Order Structure. *Chromosoma* **2009**, *118*, 537–548.
38. Ji, J.Y.; Lee, R.T.; Vergnes, L.; Fong, L.G.; Stewart, C.L.; Reue, K.; Young, S.G.; Zhang, Q.; Shanahan, C.M.; Lammerding, J. Cell Nuclei Spin in the Absence of Lamin b1. *J. Biol. Chem.* **2007**, *282*, 20015–20026.
39. Fais, D.; Prusov, A.N.; Polyakov VYu The Anchorosome, a Special Chromatin Granule for the Anchorage of the Interphase Chromosome to the Nuclear Envelope. *Cell Biol. Int. Rep.* **1989**, *13*, 747–758.
40. Olins, A.L.; Buendia, B.; Herrmann, H.; Lichter, P.; Olins, D.E. Retinoic Acid Induction of Nuclear Envelope-Limited Chromatin Sheets in HL-60. *Exp. Cell Res.* **1998**, *245*, 91–104.
41. Davies, H.G. Electron-Microscope Observations on the Organization of Heterochromatin in Certain Cells. *J. Cell Sci.* **1968**, *3*, 129–150.
42. Ghadially, F.N. Nucleus. In *Ultrastructural Pathology of the Cell and Matrix*; Elsevier, 1988; pp. 1–180 ISBN 9780407015715.
43. Olins, A.L.; Ishaque, N.; Chotewutmontri, S.; Langowski, J.; Olins, D.E. Retrotransposon Alu Is Enriched in the Epichromatin of HL-60 Cells. *Nucleus* **2014**, *5*, 237–246.
44. Xu, P.; Mahamid, J.; Dombrowski, M.; Baumeister, W.; Olins, A.L.; Olins, D.E. Interphase Epichromatin: Last Refuge for the 30-Nm Chromatin Fiber? *Chromosoma* **2021**, *130*, 91–102.
45. Erenpreisa, J.; Ivanov, A.; Cragg, M.; Selivanova, G.; Illidge, T. Nuclear Envelope-Limited Chromatin Sheets Are Part of Mitotic Death. *Histochem. Cell Biol.* **2002**, *117*, 243–255.
46. Celli, G.B.; Denchi, E.L.; de Lange, T. Ku70 Stimulates Fusion of Dysfunctional Telomeres yet Protects Chromosome Ends from Homologous Recombination. *Nat. Cell Biol.* **2006**, *8*, 885–890.
47. Paddock, S.W.; Albrecht-Buehler, G. Rigidity of the Nucleus during Nuclear Rotation in 3T3 Cells. *Exp. Cell Res.* **1988**, *175*, 409–413.

48. Franklin, R.E.; Gosling, R.G. Molecular Configuration in Sodium Thymonucleate. *Nature* **1953**, *171*, 740–741.
49. Erenpreisa, J.; Krigerts, J.; Salmina, K.; Selga, T.; Sorokins, H.; Freivalds, T. Differential Staining of Peripheral Nuclear Chromatin with Acridine Orange Implies an A-Form Epichromatin Conformation of the DNA. *Nucleus* **2018**, *9*, 171–181.
50. Erenpreisa, J.; Salmina, K.; Krigerts, J.; Selga, T.; Freivalds, T. The Nuclear Envelope-Associated Epichromatin and Its Sheets Are Composed of DNA A-Form Packed as Nucleosomal Superbeads Which Construct Vehicles for the Gear-Wheel Nuclear Traffic. *Biopolym. Cell* **2019**, *35*, 167–167.
51. Erenpreisa, J.; Huna, A.; Salmina, K.; Jackson, T.R.; Cragg, M.S. Macroautophagy-Aided Elimination of Chromatin: Sorting of Waste, Sorting of Fate? *Autophagy* 2012, *8*, 1877–1881.
52. Olins, A.L.; Langhans, M.; Monestier, M.; Schlotterer, A.; Robinson, D.G.; Viotti, C.; Zentgraf, H.; Zwerger, M.; Olins, D.E. An Epichromatin Epitope: Persistence in the Cell Cycle and Conservation in Evolution. *Nucleus* **2011**, *2*, 47–60.
53. Gould, T.J.; Tóth, K.; Mücke, N.; Langowski, J.; Hakusui, A.S.; Olins, A.L.; Olins, D.E. Defining the Epichromatin Epitope. *Nucleus* **2017**, *8*, 625–640.
54. Teif, V.B.; Mallm, J.-P.; Sharma, T.; Mark Welch, D.B.; Rippe, K.; Eils, R.; Langowski, J.; Olins, A.L.; Olins, D.E. Nucleosome Repositioning during Differentiation of a Human Myeloid Leukemia Cell Line. *Nucleus* **2017**, *8*, 188–204.
55. Cebrián-Silla, A.; Alfaro-Cervelló, C.; Herranz-Pérez, V.; Kaneko, N.; Park, D.H.; Sawamoto, K.; Alvarez-Buylla, A.; Lim, D.A.; García-Verdugo, J.M. Unique Organization of the Nuclear Envelope in the Post-Natal Quiescent Neural Stem Cells. *Stem Cell Reports* **2017**, *9*, 203–216.
56. Vicari, M.R.; Bruschi, D.P.; Cabral-de-Mello, D.C.; Nogaroto, V. Telomere Organization and the Interstitial Telomeric Sites Involvement in Insects and Vertebrates Chromosome Evolution. *Genet. Mol. Biol.* **2022**, *45*, e20220071.
57. Baker, D.J.; Sedivy, J.M. Probing the Depths of Cellular Senescence. *J. Cell Biol.* 2013, *202*, 11–13.
58. Boateng, K.A.; Bellani, M.A.; Gregoretti, I.V.; Pratto, F.; Camerini-Otero, R.D. Homologous Pairing Preceding SPO11-Mediated Double-Strand Breaks in Mice. *Dev. Cell* **2013**, *24*, 196–205.
59. Prieler, S.; Chen, D.; Huang, L.; Mayrhofer, E.; Zsótér, S.; Vesely, M.; Mbogning, J.; Klein, F. Spo11 Generates Gaps through Concerted Cuts at Sites of Topological Stress. *Nature* **2021**, *594*, 577–582.
60. Wang, J.; Zhang, L.; Wang, J.; Hao, Y.; Xiao, Q.; Teng, J.; Shen, S.; Zhang, Y.; Feng, Y.; Bao, S.; et al. Conversion between Duplicated Genes Generated by Polyploidization Contributes to the Divergence of Poplar and Willow. *BMC Plant Biol.* **2022**, *22*, 298.
61. Maciver, S.K.; Koutsogiannis, Z.; de Obeso Fernández Del Valle, A. "Meiotic Genes" Are Constitutively Expressed in an Asexual Amoeba and Are Not Necessarily Involved in Sexual Reproduction. *Biol. Lett.* **2019**, *15*, 20180871.
62. Bailey, J.A.; Eichler, E.E. Primate Segmental Duplications: Crucibles of Evolution, Diversity and Disease. *Nat. Rev. Genet.* **2006**, *7*, 552–564.
63. Yi, J.; Yeou, S.; Lee, N.K. DNA Bending Force Facilitates Z-DNA Formation under Physiological Salt Conditions. *J. Am. Chem. Soc.* **2022**, *144*, 13137–13145.
64. Shubernetskaya, O.; Skvortsov, D.; Evfratov, S.; Rubtsova, M.; Belova, E.; Strelkova, O.; Cherepaninets, V.; Zhironkina, O.; Olovnikov, A.; Zvereva, M.; et al. Interstitial Telomeric Repeats-Associated DNA Breaks. *Nucleus* **2017**, *8*, 641–653.
65. Herbert, A. ALU Non-B-DNA Conformations, Flipons, Binary Codes and Evolution. *R Soc Open Sci* **2020**, *7*, 200222.
66. Bosco, N.; de Lange, T. A TRF1-Controlled Common Fragile Site Containing Interstitial Telomeric Sequences. *Chromosoma* **2012**, *121*, 465–474.
67. Zaitceva, V.; Kopeina, G.S.; Zhivotovsky, B. Anastasis: Return Journey from Cell Death. *Cancers* **2021**, *13*, doi:10.3390/cancers13153671.
68. Mardin, B.R.; Drainas, A.P.; Waszak, S.M.; Weischenfeldt, J.; Isokane, M.; Stütz, A.M.; Raeder, B.; Efthymiopoulos, T.; Buccitelli, C.; Segura-Wang, M.; et al. A Cell-Based Model System Links Chromothripsis with Hyperploidy. *Mol. Syst. Biol.* **2015**, *11*, 828.
69. Cortés-Ciriano, I.; Lee, J.J.-K.; Xi, R.; Jain, D.; Jung, Y.L.; Yang, L.; Gordenin, D.; Klimczak, L.J.; Zhang, C.-Z.; Pellman, D.S.; et al. Comprehensive Analysis of Chromothripsis in 2,658 Human Cancers Using Whole-Genome Sequencing. *Nat. Genet.* **2020**, *52*, 331–341.
70. Bassaganyas, L.; Beà, S.; Escaramís, G.; Tornador, C.; Salaverria, I.; Zapata, L.; Drechsel, O.; Ferreira, P.G.; Rodriguez-Santiago, B.; Tubio, J.M.C.; et al. Sporadic and Reversible Chromothripsis in Chronic Lymphocytic Leukemia Revealed by Longitudinal Genomic Analysis. *Leukemia* **2013**, *27*, 2376–2379.
71. Ye, C.J.; Liu, G.; Heng, H.H. Experimental Induction of Genome Chaos. *Methods Mol. Biol.* **2018**, *1769*, 337–352.

72. Hu, Q.; Valle-Inclan, J.E.; Dahiya, R.; Guyer, A.; Mazzagatti, A.; Maurais, E.G.; Engel, J.L.; Cortés-Ciriano, I.; Ly, P. Non-Homologous End Joining Shapes the Genomic Rearrangement Landscape of Chromothripsis from Mitotic Errors. *bioRxiv* **2023**, doi:10.1101/2023.08.10.552800.
73. Comaills, V.; Castellano-Pozo, M. Chromosomal Instability in Genome Evolution: From Cancer to Macroevolution. *Biology* **2023**, *12*, doi:10.3390/biology12050671.
74. Erenpreisa, J.; Vainshelbaum, N.M.; Lazovska, M.; Karklins, R.; Salmina, K.; Zayakin, P.; Rumnieks, F.; Inashkina, I.; Pjanova, D.; Erenpreiss, J. The Price of Human Evolution: Cancer-Testis Antigens, the Decline in Male Fertility and the Increase in Cancer. *Int. J. Mol. Sci.* **2023**, *24*, doi:10.3390/ijms241411660.
75. Weinberg, R.A. Coming Full Circle-from Endless Complexity to Simplicity and Back Again. *Cell* **2014**, *157*, 267–271
76. Erenpreisa, J.; Giuliani, A. Resolution of Complex Issues in Genome Regulation and Cancer Requires Non-Linear and Network-Based Thermodynamics. *Int. J. Mol. Sci.* **2019**, *21*, doi:10.3390/ijms21010240]
77. .McCLINTOCK, B. The Origin and Behavior of Mutable Loci in Maize. *Proc. Natl. Acad. Sci. U. S. A.* **1950**, *36*, 344–355.